PERGAMON

Chemical Engineering Science 57 (2002) 1459–1474

Chemical Engineering Science

www.elsevier.com/locate/ces

Spatiotemporal patterns within a porous catalyst: dynamic carbon monoxide oxidation in a single-pellet reactor

Laura C. Nett-Carrington, Richard K. Herz *

Department of Mechanical and Aerospace Engineering, Chemical Engineering Program, University of California at San Diego, 9500 Gilman Drive, San Diego, CA 92093-0411, USA

Received 16 June 2000; accepted 10 January 2002

Abstract

Competitive adsorption and reactant inhibition are expected to couple with diffusion resistance to form complex patterns within porous adsorbents and catalysts, especially under dynamic conditions. CO oxidation over Pt/Al_2O_3, which exhibits these surface processes, was studied in this work. A miniaturized single-pellet reactor was used to continuously and directly measure gas concentration gradients within a porous pellet as feed composition was varied. Responses of nonadsorbing species were analyzed in order to determine diffusion coefficients. Single-species responses provided starting estimates of CO adsorption parameters. Reaction experiments were performed at 398–448 K under maximum CO and O_2 pressures of 16 and 110 Pa, respectively. An elementary-step diffusion–reaction model was used to simulate experimental results. A bimodal distribution of active sites was proposed in order to explain the transient responses. Analysis showed that the bimodal distribution could not have been detected by steady-state experiments. The intrapellet spatiotemporal patterns predicted by the model, and confirmed by comparison to measurements of concentration gradients across the pellet, provide understanding of the dynamic coupling between diffusion, adsorption, and reaction within the pellet. Methods are discussed to reduce computational requirements, including assumption of quasi-equilibrium adsorption, and reduction of the surface-to-gas capacity ratio.

Keywords: Kinetics; Nonlinear dynamics; Reaction engineering; Transient response; Catalysis; Porous media

1. Introduction

Transport processes and surface reactions can interact in complex ways during unsteady-state, dynamic, operation of porous adsorbents and catalysts. Dynamic operation is encountered in processes such as temperature- and pressure-swing adsorbers (Keller II, 1995), automotive catalysts (Herz, 1987; Farrauto & Heck, 1999), and catalytic reactors that are deliberately operated under periodic conditions for enhanced performance (Zagoruiko, Matros, Kumar, & Kulkarni, 1992; Silveston, Hudgins, Bogdashev, Vernijakovskaja, & Matros, 1994; Khadilkar, Al-Dahhan, & Dudukovic, 1998; Jirát, Stepánek, Kubícek, & Marek, 1998). In the laboratory, transient kinetic techniques are used to study porous adsorbents and catalysts in order to obtain information such as quantities of species adsorbed (Kobayashi, Maeda, & Takahashi, 1983; Tamaru, 1991; Dogu, Yasyerli, Mccoy, & Smith, 1996).

Analysis of these systems is hampered by the difficulty of measuring thermal and concentration patterns as they evolve inside the porous solids. This work demonstrates how concentration gradients that result from diffusion resistance can be measured experimentally and then analyzed with detailed numerical simulations. The results of these measurements and simulations reveal the spatiotemporal patterns that form inside the porous solids and provide understanding of how diffusion and surface reactions couple under dynamic conditions.

The system studied here is the reaction between CO and O_2 to form CO_2 over porous Pt/Al_2O_3. This reaction, especially its temperature dependence at low temperature, is important in control of emissions from combustion processes. CO oxidation also can be considered a model reaction that exhibits many important characteristics of surface reactions (Cannestra, Nett, & Herz, 1997). The autocatalytic nature of the reaction is expected to exhibit spatial structures of

* Corresponding author. Tel.: +1-858-534-6540; fax: +1-858-534-4543.
E-mail address: herz@ucsd.edu (R. K. Herz).

0009-2509/02/$ - see front matter
PII: S0009-2509(02)00046-5

adsorbed species within a porous catalyst (Hlavacek & Van Rompay, 1981), and this work provides experimental confirmation of these structures.

The reaction feature of primary interest here is the accumulation of adsorbed CO within the porous catalyst. CO competes with O_2 for adsorption sites and tends to win this competition at low temperatures and during periods when the CO/O_2 ratio is high. The accumulated CO inhibits the reaction rate and affects the dynamic response of the system. We are interested in learning how CO penetrates into the porous catalyst and accumulates, how accumulated CO is removed during periods of low CO/O_2 ratio, and how these processes are affected by diffusion resistance and how they change with temperature. The qualitative results of this work are applicable to other catalytic reactions in which competitive adsorption and reactant inhibition are important.

The catalyst studied was in the form of a thin, disk-shaped pellet of $Pt/Al_2\ O_3$. The sample was contained within a form of single-pellet diffusion reactor (Au, Dranott, & Butt, 1995; Hegedus & Petersen, 1974) that allows continuous, direct measurement of gas concentration gradients within the pellet as the composition of the feed is varied.

A detailed model of diffusion and reaction is developed and used to simulate the experimental responses. No assumptions are made about a rate-limiting step, and individual adsorption, desorption, and reaction steps are described separately. With confidence in the model enhanced by its ability to fit experimental measurements at the pellet's external face and center, the model can be used to show the spatiotemporal patterns that developed within the pellet and can be used to answer questions about diffusion resistance and transient CO accumulation.

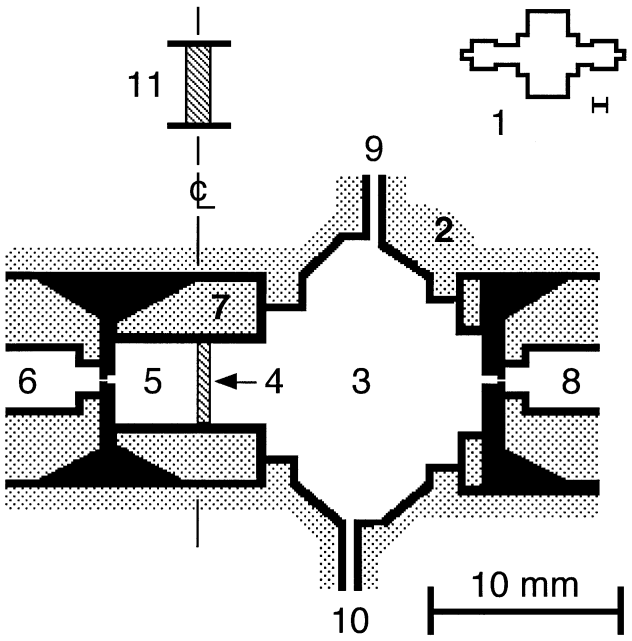

Fig. 1. Schematic cross-section of reactor. (1) Outline of reactor body. Scale bar to lower right of outline is 10 mm. Positions 2–10 are located at center of reactor body. Reactor has cylindrical symmetry about the horizontal axis through positions 3–6. (2) Stainless steel body of reactor. (3) Bulk chamber though which reactant gas flows. (4) Bulk (exterior) face of porous catalyst pellet. Pellet is a thin cylindrical disk with its circumference sealed against the pellet holder and its circular faces exposed to gas in the bulk and centerplane chambers. (5) Centerplane chamber. (6) Pinhole leak from centerplane chamber to mass spectrometer. (7) Pellet holder. (8) Leak from bulk chamber to mass spec. Black triangles between positions 6–7 and 2–8 are O-ring seals. (9) Reactant gas inlet to bulk chamber. (10) Reactant and product gas outlet from bulk chamber. Positions 9–10 are ports spaced alternately around circumference of bulk chamber. (11) Illustration, not part of apparatus, of a full pellet. The sample pellet is equivalent to the right half of this full pellet in the limit of zero centerplane chamber volume and leak.

2. Experimental

A cross-section of the core of the reactor is shown in Fig. 1. Details of the apparatus, as well as a discussion of the relationships of this reactor to other single-pellet apparatuses, are given in Cannestra et al. (1997). The volumes of the bulk chamber and the centerplane chamber are 5.6×10^{-7} m^3 (0.56 cm^3) and 4.4×10^{-8} m^3 (0.044 cm^3), respectively. The catalyst pellet, located at position 4 in the figure, was pressed from Pt/Al_2O_3 powder into position in the pellet holder, forming a porous disk 4 mm in diameter and 0.64 mm in thickness. The pellet is equivalent to the right half of the full pellet at position 11 in the figure, in the limit of zero centerplane chamber volume and leak rate. The 2 wt%-Pt powder was prepared from chloroplatinic acid and transitional-phase alumina (Racine & Herz, 1992) and had a dispersion of 1%, as used in this work and as determined in the adsorption and reaction response experiments described below.

Experiments were conducted with total gas pressures over the pellet of up to 350 Pa (1 Pa = 1 N/m^2 = 10^{-5} atm = 0.76×10^{-2} Torr). Temperatures ranged from 398 to 448 K. At 100 Pa and 423 K, the mean free path of CO and O_2 is 10^{-4} m. As a result, under the conditions used in this work, laminar and transitional gas flow occurred in the flow passages of the reactor, whereas molecular flow, or Knudsen diffusion, occurred in the pellet pores and through the bulk and centerplane leaks to the mass spectrometer. The leaks were laser-drilled pinholes in 1.3×10^{-5} m-thick metal foil, with hole diameters of 1.5×10^{-5} m (bulk leak) and 3×10^{-6} m (centerplane).

The mean residence time of gas flowing through the bulk chamber was 0.2 s in this work. The gas in both the bulk and centerplane chambers are mixed rapidly by diffusion. For example, at 200 Pa and 423 K, the diffusivity of CO in O_2 is 1.8×10^{-2} m^2/s. Since the diameter of the bulk chamber is 1×10^{-2} m and the diameter of the centerplane chamber is 0.4×10^{-2} m, the time constants for diffusive mixing in the chambers are $\leqslant 6 \times 10^{-3}$ s. Gas mixtures contained one or both of the inert gases Ne and Ar in order to aid in resetting mass spectrometer sensitivity and in order to provide inert

responses to compare with adsorption and reaction responses measured during the same experiment.

Cannestra et al. (1997) demonstrated that the accumulation of gas in the centerplane chamber and the leak of gas from the chamber are small such that conditions at the centerplane face of the pellet closely approximates the zero-flux condition at the center of a full pellet. The perturbations from the zero flux condition can be accurately accounted for in mathematical models of the system and, thus, introduce no uncertainties in the analysis.

Measurement of gas composition on both sides of the pellet provides direct measurement of the effects of diffusion resistance in the pellet. Several types of experiments can be performed with the apparatus:

- dynamic inert response to obtain diffusion coefficients,
- dynamic adsorption–desorption response,
- reaction under steady-state and dynamic conditions.

3. Model equations

3.1. Detailed models of CO oxidation in porous catalysts

In early work, Herz and Marin (1980) fit an elementary-step, detailed, model of CO oxidation to steady-state measurements over Pt/Al_2O_3. Diffusion effects were accounted for indirectly using an effectiveness factor. Elementary-step CO oxidation models fit to transient experimental data, but without a description of intrapellet diffusion, include the works of Graham and Lynch (1987), Wolf and students (Kaul, Sant, & Wolf, 1987; Sant & Wolf, 1990), Marin and students (Hoebink, Huinink, & Marin, 1997; Hoebink, Nievergeld, & Marin, 1999), and Dekker, Klopper, Bliek, Kapteijn, & Moulijn (1994).

Cho (1983) presented simulations computed from a detailed model of diffusion and surface reactions for CO oxidation in a porous catalyst under dynamic conditions. Time-resolved experimental measurements were not available for comparison in that work. The addition of diffusion to reaction models significantly increases computational demands (Hindmarsh & Johnson, 1991). In more recent work, detailed diffusion–reaction models have been compared to time-resolved experimental data. Racine and Herz (1992) fit a detailed reaction–diffusion model to time-resolved measurements of CO oxidation over a porous Pt/Al_2O_3 pellet. Hoebink et al. (1997) used a detailed model of reaction with diffusion down a bed of nonporous Pt powder particles to fit time-resolved measurements in a type of evacuated pulse microreactor, or "temporal analysis of products (TAP)" reactor (Gleaves, Ebner, & Kuechler, 1988). Those experiments involved sequentially pulsing CO and O_2 at one end of the bed and measuring unconverted reactant and the reaction product CO_2 diffusing out the evacuated end of the bed. The equations for this later system, where flow is solely by Knudsen diffusion, are similar to those for diffusion and reaction in a one-dimensional porous pellet, differing mainly in the boundary conditions.

3.2. Gas in pellet pores

The conservation equations that form the framework of the numerical models are shown in this section. The functional forms of the rate terms r_i are given below in Sections 5 and 6. Conditions within the pellet are nearly isothermal during experiments shown here and isothermal conditions are specified in the model. Conditions are assumed to be uniform radially in the pellet and the pellet is specified to be a one-dimensional system. The conservation equations for the gaseous species in the pellet pores are given by

$$\frac{\partial \Psi_i}{\partial t} = \frac{1}{\tau_i}\left(\frac{\partial^2 \Psi_i}{\partial \lambda^2}\right) + \alpha_i(-r_i^{\mathrm{ads}} + r_i^{\mathrm{des}}), \tag{1}$$

where subscript i is the species index, as appropriate for the type of experiment. For example, for CO oxidation experiments, the gas species are CO, O_2 and CO_2, and equations for each of these species are written and integrated. Time t (s) is not made dimensionless, and each group of terms has units of s^{-1}. The dimensionless position variable is λ, with $\lambda = 0$ at the centerplane face of the pellet and $\lambda = 1$ at the bulk (exterior) face. For making concentrations dimensionless, j is a species index, where $j = \mathrm{CO}$ for $i = \mathrm{CO}$ and CO_2 and where $j = O_2$ for $i = O_2$.

$$\Psi_i = \frac{C_i}{C_j^{\max}}, \tag{2}$$

$$\tau_i = \left(\frac{\varepsilon L^2}{D_i^{\mathrm{eff}}}\right), \tag{3}$$

$$\alpha_i = \left(\frac{C_{\mathrm{tot}}^{\mathrm{surf}}}{\varepsilon C_j^{\max}}\right). \tag{4}$$

The C_i are the concentrations of gas-phase species. The void fraction of the pellet, $\varepsilon = 0.3$, was determined by mercury porosity measurements on separate pellets pressed using the same procedure. The thickness of the sample pellet is L (0.64 mm). τ_i is the characteristic time for diffusion in the pellet in absence of adsorption. In all experiments in this work, pressures were low such that Knudsen diffusion was the only mode of diffusion in the pellet pores. Because of this, diffusion coefficients were independent of pressure. The effective diffusion coefficient ($m^2\ s^{-1}$) for species i in the pellet is given by

$$D_i^{\mathrm{eff}}(T) = D_{\mathrm{CO}}^{\mathrm{eff}}\ (300\ \mathrm{K})\left(\frac{T}{300\ \mathrm{K}}\right)^{0.5}\left(\frac{M_{\mathrm{CO}}}{M_i}\right)^{0.5}, \tag{5}$$

T is temperature and M_i is the molecular weight of species i. The surface-to-gas capacity ratio is α_i. This is the ratio between the maximum number of moles that can be adsorbed

on the surface to the maximum number of moles of gas that can be held in the pore volume of the pellet. $C_{\text{tot}}^{\text{surf}}$ is the total moles of surface Pt atoms per unit volume of pellet.

3.3. Surface species

The pore gas equations are coupled to conservation equations for adsorbed CO molecules and O atoms through the adsorption and desorption rates. At each position λ,

$$\left(\frac{\partial \Theta_{n\text{CO}}}{\partial t} = r_{n\text{CO}}^{\text{ads}} - r_{n\text{CO}}^{\text{des}} - r_n^{rxn}\right)_{\lambda}, \tag{6}$$

$$\left(\frac{\partial \Theta_{n\text{O}}}{\partial t} = 2r_{n\text{O}_2}^{\text{ads}} - 2r_{n\text{O}_2}^{\text{des}} - r_n^{rxn}\right)_{\lambda}, \tag{7}$$

where n is the index for different adsorption site types for heterogeneous surfaces. CO_2 response experiments demonstrated that CO_2 did not adsorb to an appreciable extent and an equation for adsorbed CO_2 was not written. Dimensionless surface concentrations, or fractional surface coverages, are defined by

$$\Theta_{nk} = \frac{C_{nk}^{\text{surf}}}{\phi_n C_{\text{tot}}^{\text{surf}}}, \tag{8}$$

where k is the adsorbed species index, and ϕ_n is the fraction of surface Pt atoms that are of site type n. Each r in the gas equations equals the sum over n of r_n. Equations for the individual rates are given in the sections below describing each type of experiment.

3.4. Boundary and initial conditions

The boundary conditions for the pore gas equations, Eq. (1) are

$$\begin{aligned} &\Psi_i = \text{experimentally measured } \Psi_i \quad \text{at } \lambda = 1 \\ &\Psi_i = \Psi_i^{cp} \qquad\qquad\qquad\quad \text{at } \lambda = 0 \end{aligned} \quad \text{for } t \geqslant 0, \tag{9}$$

where the Ψ_i^{cp} are the dimensionless gas-phase concentrations in the centerplane chamber. The Ψ_i^{cp} are computed by solving the following equations for the centerplane chamber simultaneously with the pore gas and surface equations:

$$\frac{\partial \Psi_i^{cp}}{\partial t} = \frac{1}{\tau_i^{cpp}}\left(\left.\frac{\partial \Psi_i}{\partial \lambda}\right|_{\lambda=0}\right) - \frac{\Psi_i^{cp}}{\tau_i^{cpl}}, \tag{10}$$

$$\Psi_i^{cp} = \frac{C_i^{cp}}{C_j^{\max}}, \tag{11}$$

$$\tau_i^{cpp} = \frac{V^{cp}L}{D_i^{\text{eff}}A}, \tag{12}$$

$$\tau_i^{cpl} = \frac{V^{cp}}{Q_i^{cpl}}, \tag{13}$$

τ_i^{cpp} is the characteristic time of filling the centerplane chamber by gas diffusing into the chamber from the pellet. τ_i^{cpl} is the characteristic time of emptying the centerplane chamber by gas leaving through the sample leak. V^{cp} is the volume of the centerplane chamber (4.4×10^{-8} m^3). A is the area of each face of the pellet (1.26×10^{-5} m^2). Q_i^{cpl} is the "pumping speed" of the sample leak from the centerplane chamber for species i

$$Q_i^{cpl}(T) = Q_{\text{CO}}^{cpl}\ (300\ \text{K})\left(\frac{T}{300}\right)^{0.5}\left(\frac{M_{\text{CO}}}{M_i}\right)^{0.5}, \tag{14}$$

where $Q_{\text{CO}}^{cpl}\ (300\ \text{K}) = 1.9 \times 10^{-10}$ m^3 s^{-1} was calculated using relationships for molecular flow through a short tube of the dimensions of the sample leak.

The first group of terms on the right-hand side (RHS) of Eq. (10) is the rate at which the species diffuses from the pellet into the centerplane chamber. The second group of terms on the RHS is the rate at which the species flows out of the centerplane chamber through the small hole to the mass spectrometer.

For the CO oxidation experiments, the initial conditions are

$$\begin{aligned} &\Psi_{\text{CO}}(\lambda) = \Psi_{\text{CO}_2}(\lambda) \\ &\qquad = \Psi_{\text{CO}}^{cp} = \Psi_{\text{CO}_2}^{cp} = 0 \\ &\Psi_{O_2}(\lambda) = \Psi_{O_2}^{cp} = 1 \qquad\qquad \text{at } t = 0 \text{ for } 0 < \lambda < 1, \\ &\Theta_{n\text{CO}}(\lambda) = 1 \times 10^{-16} \\ &\Theta_{n\text{O}}(\lambda) = 0.5 \end{aligned} \tag{15}$$

The surface coverage of CO is set to a small nonzero value for computational stability at early time. The surface coverage of adsorbed oxygen atoms is set to its specified maximum value. CO_2 is specified to adsorb in negligible amounts, so the desorption rate of CO_2 is set equal to its formation rate in the pore gas equation for CO_2 and the surface conservation equation for CO_2 is neglected.

The equations are integrated and parameter values are adjusted between integration runs to minimize the difference between the computed Ψ_i^{cp} and the experimentally measured Ψ_i^{cp}.

4. Inert response—results and discussion

Inert responses are analyzed in order to determine the values of effective diffusion coefficients in the sample pellet. The diffusion coefficients were then used in the analysis of adsorption and reaction response experiments performed with the same pellet.

In one type of inert response experiment, Ne or Ar was turned on and off periodically in the feed to the system. The cycling periods were long such that steady state was reached after each change in inert concentration. Since Ar was present in the CO feed for CO oxidation reaction experiments, this type of inert response analysis could also be performed for each reaction experiment.

In the second type of experiment, the Pt in the pellet was saturated with CO at a relatively low temperature, 308 K,

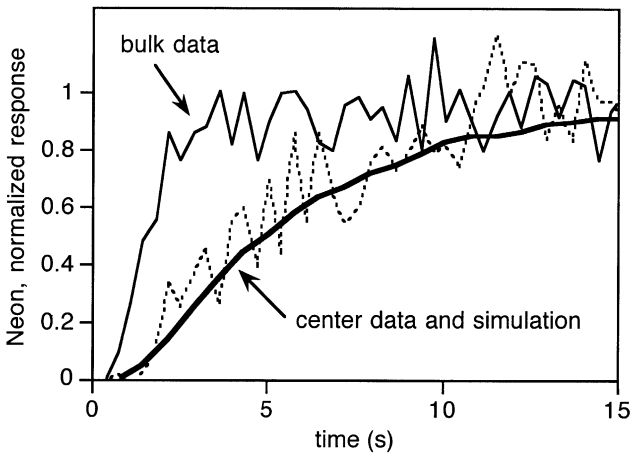

Fig. 2. Response of Ne diffusion through pellet at 308 K. The simulation curve was computed by numerically integrating Eqs. (1) and (10) for one species, with the reaction rate terms r_i set to zero.

then the CO flow to the system was turned on and off periodically. Because the desorption rate was slow such that adsorption sites in the pellet were nearly saturated with CO at all times, the gas-phase CO diffused in the pellet without interacting noticeably with the surface.

In the system of equations describing these inert response experiments, all r_{ni} are set to zero and the surface species equations are not involved. For the one species, Eq. (1) and Eq. (10) are solved using the numerical method of lines with a three-point approximation in space and a fifth-order Runge–Kutta–Fehlberg method of integration in time. D_i^{eff} is determined by integrating the equations and then adjusting the value of D_i^{eff} in order to match the simulated to the measured centerplane concentrations.

Fig. 2 shows results of an experiment at 308 K using Ne. Data for one cycle during periodic cycling are shown. The centerplane response was fit with $D_{\text{Ne}}^{\text{eff}} = 4.0 \times 10^{-7}\ \text{m}^2\ \text{s}^{-1}$. Applying a void fraction of 0.3 and a tortuosity of 3 to the Knudsen diffusion coefficient for a straight cylindrical pore, this value of $D_{\text{Ne}}^{\text{eff}}$ would be obtained with a porous material having a uniform pore diameter of 20 nm. The Al_2O_3 support used here has 45% of the pore volume as macropores with an average pore diameter of 500 nm and the balance as micropores with an average pore diameter of 8 nm, so the $D_{\text{Ne}}^{\text{eff}}$ value obtained is physically reasonable.

The effective diffusivity of CO at reaction temperatures was estimated by two methods. In one, the value of $D_{\text{CO}}^{\text{eff}}$ measured at 308 K was corrected to reaction temperature by using the dependence of Knudsen diffusivity on temperature. In the other method, $D_{\text{CO}}^{\text{eff}}$ at the reaction temperature was estimated from the effective diffusivity of Ne and Ar at reaction temperature using the dependence of Knudsen diffusion on molecular weight. Both methods gave the same result, and $D_{\text{CO}}^{\text{eff}}\ (300\ \text{K}) = 4.0 \times 10^{-7}\ \text{m}^2\ \text{s}^{-1}$ in Eq. (5).

The system response in this experiment is dominated by filling of the centerplane chamber. The characteristic time for inert gas diffusion in the pores, τ_i, is about 0.3 s, which is not greatly larger than the time resolution of the current measurement system, about 0.1 s. If the centerplane chamber volume were zero, the inert response at the centerplane would be too fast to measure accurately. However, with the current size of the chamber, filling of the chamber is relatively slow and can be measured accurately. The response can be fit reasonably well with a model that specifies that inert gas diffusion in the pores is in quasi-steady state. In such a model, the characteristic response time constant, τ_i^{cpp}, has a value of about 5.6 s. Since the values of V^{cp}, L, A and τ_i^{cpp} are known in Eq. (12), the value of the effective diffusion coefficient D_i^{eff} can be determined accurately. This requirement of a relatively large centerplane chamber volume for inert-response experiments contrasts with the desire for a very small volume in adsorption and reaction experiments. A nonzero volume is required in all types of experiments, since the sampling method of a point gas leak requires a nonzero volume to allow gas collection from the entire face of the pellet, such that the sample leak rate is much less than the diffusion rate through the pellet face. The current centerplane chamber volume is a reasonable balance between these competing design requirements.

5. Adsorption response—results and discussion

Adsorption–desorption responses can be analyzed in order to fit adsorption isotherms and, in favorable cases, the values of adsorption and desorption rate coefficients. With accurate measurement of feed flow rate and the use of an inert tracer in the feed, transient species balances can be made and used to determine a sample's capacities for adsorbed species.

In the experiments reported here, CO was turned on and off periodically in the feed to the system. Temperatures were greater than 308 K such that CO adsorbed and desorbed at appreciable rates and the surface coverage by CO changed appreciably. The cycling periods were long such that steady state was reached after each change in CO pressure. Fig. 3 shows data for a CO response experiment. Bulk and centerplane CO pressure data are shown for a single cycle during periodic switching of the feed CO on and off.

To simulate the experiment, Eqs. (1), (6), and (10) for the single species CO were integrated numerically using the Crank–Nicolson method (Crank & Nicolson, 1947). This finite-difference method is second-order accurate in both space and time, implicit in time, and unconditionally stable (Pozrikidis, 1998). The time steps were adaptive in order to keep changes in dependent variables within specified ranges. The rate terms in Eqs. (1) and (6) for CO adsorption and desorption were specified to have first-order kinetics in this model.

CO *adsorption*

$$(*) + \text{CO(g)} \rightarrow (*)\text{–CO},$$

$$r_{\text{CO}}^{\text{ads}} = k_{\text{CO}}^{\text{ads}} C_{\text{CO}}^{\max} \Psi_{\text{CO}} (1 - \Theta_{\text{CO}}). \tag{16}$$

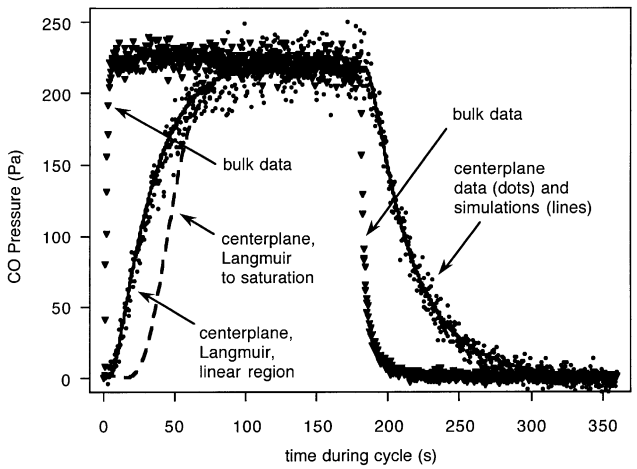

Fig. 3. Response of CO diffusion and adsorption in pellet at 423 K. The simulation curve was computed by numerically integrating Eqs. (1), (6), and (10) for one species and one surface site type. The reaction term r^{rxn} was set to zero and the r^{ads} and r^{des} terms are given by Eqs. (16) and (17).

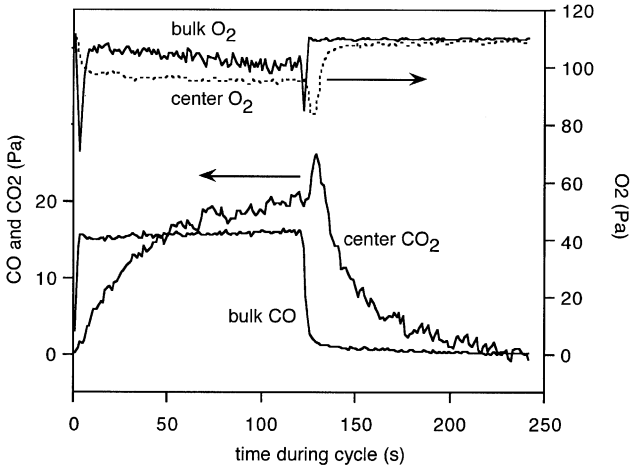

Fig. 4. Data measured as feed CO was periodically switched on and off in a constant flow of O_2 at 423 K. A single, averaged cycle is shown in this figure and following figures with similar data.

CO *desorption*

$$(*)\text{–CO} \rightarrow (*) + \text{CO(g)},$$

$$r_{CO}^{des} = k_{CO}^{des}\Theta_{CO}. \tag{17}$$

The (*) represents a surface site for CO adsorption. The rate coefficient k_{CO}^{ads} ($m^3\ mol^{-1}\ s^{-1}$) is equal to the collision frequency (s^{-1}) of gaseous CO molecules with Pt surface atoms at a given gaseous CO concentration divided by that concentration (mol m^{-3}) and finally multiplied by the sticking probability of a molecule of CO on the clean surface, S_{CO}^{ads}:

$$k_{CO}^{ads} = \left(\frac{RT}{2\pi M_{CO}}\right)^{0.5} \sigma S_{CO}^{ads}, \tag{18}$$

where σ is the area occupied by 1 mol of surface Pt atoms $= 5.5 \times 10^4\ m^2\ mol^{-1}$. S_{CO}^{ads} was fixed at 1.0 (Ertl, Neumann, & Striet, 1977; Lauterbach, Bonilla, & Pletcher, 1999) and k_{CO}^{des} was adjusted to fit the model predictions to the data.

Eq. (16) gives a linear decrease in CO adsorption rate with increasing surface coverage. Experimental measurements of adsorption rates usually show a nonlinear dependence, with the rate decreasing only slightly with increasing coverage at low coverages, then decreasing more rapidly as saturation coverage is approached (Kisliuk, 1957; Kisliuk, 1958; Weinberg, Comrie, & Lambert, 1976; Ertl et al., 1977). First-order kinetics were used here and in the reaction model in order to minimize adjustable parameters.

The data were fit using Eqs. (16)–(18), which describe separate adsorption and desorption steps. They could also be fit with a model in which quasi-equilibrium adsorption with an equivalent Langmuir isotherm was specified (Cannestra et al., 1997). The data were fit well with both models, so we conclude that CO adsorption equilibrium is closely approached in these experiments. This conclusion is consistent with earlier analyses of CO thermal desorption from (Herz, Kiela, & Marin, 1982) and CO diffusion and adsorption (Oh & Hegedus, 1982) in porous Pt/Al_2O_3 pellets.

6. Reaction response—results and discussion

In this type of experiment, the flow rate of O_2 through the system was held constant and feed CO was turned on and off periodically. The maximum O_2 pressure was 110 Pa and the maximum CO pressure was 16 Pa. The cycling periods were sufficiently long that steady state was closely approached before each change in CO pressure.

Fig. 4 shows measurements at 423 K. Results of an averaged cycle during periodic cycling is shown. The signal-to-noise ratio is lower for the centerplane data than for the bulk data because the centerplane leak rate was smaller than the bulk leak rate. Feed flow rates were relatively high in these experiments such that the CO_2 pressure at the bulk face was much smaller than at the centerplane. The CO pressure curve at the bulk face of the pellet is nearly a square wave. No significant penetration of CO was measured at the centerplane. Thus, there are large concentration gradients sustained within the pellet during these experiments.

The most interesting feature in these responses is the small peak in centerplane CO_2 pressure that appears at mid-cycle just after the feed CO is turned off. This mid-cycle CO_2 peak was much larger in experiments at 398 K, and was very small in experiments at 448 K. Related behavior in bulk CO_2 measurements has been observed by others (Gulari, Zhou, & Sze, 1995). Peaks in CO_2 production that occur after feed CO is turned off can be attributed to "burn off" or reaction of CO that has accumulated on the catalyst surface during the period CO feed is on. Our initial hypothesis was that the increase in size of this peak as the temperature was lowered

was due to the expected increase in equilibrium adsorption coefficient for CO and an increase in equilibrium CO coverage prior to switching the feed CO off. The modeling results discussed below show that this is only the initial step in a cascade of several processes that results in the temperature dependence of this CO_2 peak.

6.1. Rate equations

An objective of this work was to determine the simplest set of surface rate expressions required to fit the simulations to the experimental data. A single set of rate equations and parameter values were sought that fit three sets of data taken at 398, 423 and 448 K.

The strategy was to start with a simple model and to introduce complexity only as required. Values of diffusion coefficients, surface capacity, and adsorption parameters measured in the apparatus on the catalyst pellet were used where possible in the diffusion–reaction model. Starting values for other kinetic parameters were taken from the literature. The first model specified a single type of surface site, coverage-invariant parameters, and rate equations similar to those of classic Langmuir–Hinshelwood models (Herz & Marin, 1980). This model could fit the data taken at 448 K but not data taken at the two lower temperatures.

The simplest modification of the kinetic model that provided an acceptable fit of these data was specification of the presence of a bimodal distribution of sites in the catalyst. The presence of a distribution of site characteristics in supported metal catalysts is expected (Foger, 1984). In the model, the same functional forms of the rate expressions were used for each of two site types, and only the parameter values of the kinetic equations varied between the sites. A similar type of two-site model was developed by Racine and Herz (1992). In that work, only measurements over the external surface of a catalyst pellet were available, and the predictions of the centerplane concentrations of that earlier model did not show the behavior measured in the experiments discussed here.

The model assumes that both adsorbed CO and adsorbed O are distributed randomly over each type of site and that rate coefficients are coverage invariant. The kinetics for this reaction model are specified by the following:

CO *adsorption*

$$(*_n) + \mathrm{CO(g)} \rightarrow (*_n)\text{–CO},$$

$$r_{\mathrm{CO}}^{\mathrm{ads}} = \phi_1 r_{1\mathrm{CO}}^{\mathrm{ads}} + \phi_2 r_{2\mathrm{CO}}^{\mathrm{ads}},$$

$$r_{n\mathrm{CO}}^{\mathrm{ads}} = k_{n\mathrm{CO}}^{\mathrm{ads}} C_{\mathrm{CO}}^{\max} \Psi_{\mathrm{CO}} (1 - \Theta_{n\mathrm{O}} - \Theta_{n\mathrm{CO}}). \tag{20}$$

CO *desorption*

$$(*_n)\text{–CO} \rightarrow (*_n) + \mathrm{CO(g)},$$

$$r_{\mathrm{CO}}^{\mathrm{des}} = \phi_1 r_{1\mathrm{CO}}^{\mathrm{des}} + \phi_2 r_{2\mathrm{CO}}^{\mathrm{des}},$$

$$r_{n\mathrm{CO}}^{\mathrm{des}} = k_{n\mathrm{CO}}^{\mathrm{des}} \Theta_{\mathrm{CO}}. \tag{21}$$

O_2 *adsorption*

$$2[*_n] + \mathrm{O_2(g)} \rightarrow 2[*_n]\text{–O},$$

$$r_{\mathrm{O_2}}^{\mathrm{ads}} = \phi_1 r_{1\mathrm{O_2}}^{\mathrm{ads}} + \phi_2 r_{2\mathrm{O_2}}^{\mathrm{ads}},$$

$$r_{n\mathrm{O_2}}^{\mathrm{ads}} = k_{n\mathrm{O_2}}^{\mathrm{ads}} C_{\mathrm{O_2}}^{\max} \Psi_{\mathrm{O_2}} (1 - 2\Theta_{n\mathrm{O}} - \kappa\Theta_{n\mathrm{CO}})^2, \tag{22}$$

$$\kappa = \frac{1 - 2\Theta_{n\mathrm{O}}}{1 - \Theta_{n\mathrm{O}}}. \tag{23}$$

The $[*_n]$ represents a surface site for O_2 adsorption on site type n. Sites for O_2 adsorption are distinguished from sites for CO adsorption, $(*_n)$, since adsorbed O and CO are specified to occupy different areas. The model specifies that $\Theta_{n\mathrm{CO}}$ can reach a maximum value of 1.0 and that $\Theta_{n\mathrm{O}}$ can reach a maximum value of 0.5. The term $\kappa\Theta_{n\mathrm{CO}}$ in Eq. (22) represents the adsorbed CO that are not immediately adjacent to adsorbed O and, thus, that are excluding O_2 adsorption from areas on the surface not accounted for by the $2\Theta_{n\mathrm{O}}$ term.

The adsorption rate coefficient for CO is given above in Eq. (18), and the adsorption rate coefficient for O_2 is similarly defined. O_2 desorption is negligible at the temperatures of this work (Hoebink et al., 1997; Dekker et al., 1997).

CO_2 *formation reaction*

$$[*_n]\text{–O} + (*_n)\text{–CO} \rightarrow [*_n] + (*_n) + \mathrm{CO_2(g)},$$

$$r^{rxn} = \phi_1 r_1^{rxn} + \phi_2 r_2^{rxn},$$

$$r_n^{rxn} = k_n^{rxn} \Theta_{\mathrm{CO}} \Theta_{\mathrm{O}}. \tag{24}$$

Experiments with CO_2 demonstrated that CO_2 adsorption in the sample was negligible. Therefore, a surface balance similar to Eq. (6) was not written for CO_2, r^{ads} in Eq. (1) for CO_2 was set equal to zero, and r^{des} in Eq. (1) for CO_2 was set equal to r^{rxn}.

Eq. (1) for each of the three gas species, Eq. (6) for adsorbed CO, Eq. (7) for adsorbed O, and Eq. (10) for each of the three gas species were integrated. The Crank–Nicolson method was used for numerical integration. The spatial dimension was partitioned into 21 equally spaced nodes. The CO gas equation, Eq. (1) above written for CO, was the stiffest equation and required the smallest time steps. Because of this, the CO gas equation was solved separately from the other equations over a small time subinterval, and then the equations were synchronized at the end of that subinterval before the solution continued. Over each subinterval, the individual concentrations changed by less than 0.01%. This separation of the equations allowed the other equations to take larger time steps than the CO gas equation, thus, conserving CPU cycles. The time steps were adaptive in order to keep changes in dependent variables within specified ranges.

The partitioning of the equations into two sets made the system a candidate for task parallelism. The model was parallelized using message passing libraries (MPI) and run on a Cray T3E. This task parallelization was not scalable beyond

Table 1
Parameter Values

Process	Symbol	Value
O_2 *adsorption*		
site 1	$S_{1O_2}^{ads}$	5.6×10^{-4}
site 2	$S_{2O_2}^{ads}$	5.6×10^{-4}
CO *adsorption*		
site 1	S_{1CO}^{ads}	1.0
site 2	S_{2CO}^{ads}	1.0
CO *desorption*		
site 1	A_{1CO}^{des}	8.0×10^{12} s^{-1}
site 2	A_{2CO}^{des}	4.0×10^{15} s^{-1}
site 1	E_{1CO}^{des}	8.4×10^{4} J mol^{-1}
site 2	E_{2CO}^{des}	1.0×10^{5} J mol^{-1}
CO_2 *formation reaction*		
site 1	A_1^{rxn}	3.4×10^{8} s^{-1}
site 2	A_2^{rxn}	9.4×10^{5} s^{-1}
site 1	E_1^{rxn}	6.3×10^{4} J mol^{-1}
site 2	E_2^{rxn}	6.3×10^{4} J mol^{-1}
$\phi_1 = 0.15,\ \phi_2 = (1 - \phi_1),\ C_{tot}^{surf} = 0.85$ mol m^{-3}		

Values for CO at 423 K: $\alpha_{CO} = 590$, $\tau_{CO} = 0.31$ s, $\tau_{CO}^{cpp} = 5.6$ s, $\tau_{CO}^{cpl} = 190$ s, $k_{1CO}^{des} = 310$ s^{-1}, $k_{2CO}^{des} = 520$ s^{-1}, $k_1^{rxn} = 6.1$ s^{-1}, $k_2^{rxn} = 0.015$ s^{-1}. Values shown were used in numerical integration of Eqs. (1), (6), (7), and (10) for CO and oxygen and two surface site types. The reaction rate terms are given by Eqs. (20)–(24).

a few processing elements because of the way the system was partitioned. Since use of a parallel machine is usually shared, most runs were done on a single processor machine dedicated to the problem. The code was optimized for a single processor using methods including loop splitting and unrolling. The final model takes from one to four days to compute on a dedicated single 550 MHz CPU that performs two floating point operations per clock tick.

When fitting the experimental responses at 398 and 423 K, the value of D_{CO}^{eff} at 300 K determined from the inert response experiments was used without change. The value of k_{CO}^{des} obtained from the adsorption response experiments was used as the starting estimate for this parameter, and the final values obtained were within one order-of-magnitude of this value.

Table 1 lists the parameter values used to obtain the simulation results. Using the Arrhenius equation, pre-exponential factors A_n, and activation energies E_n, were determined for each k_n^{des} and k_n^{rxn} using the values of that k_n at 398 and 423 K. Using these values of A_n and E_n, the respective k_n values were calculated at 448 K. The simulation results at 448 K shown in Fig. 5 and in results presented below were obtained using these extrapolated k_n values. Hoebink et al. (1999), Guinn, Rhoades, and Herz (1997), and Russell and Ekerdt (1996) have used simultaneous nonlinear regression of data over the entire range of temperatures in order to obtain estimates of activation energies. While desirable, this method was not practical here because of the long computation times.

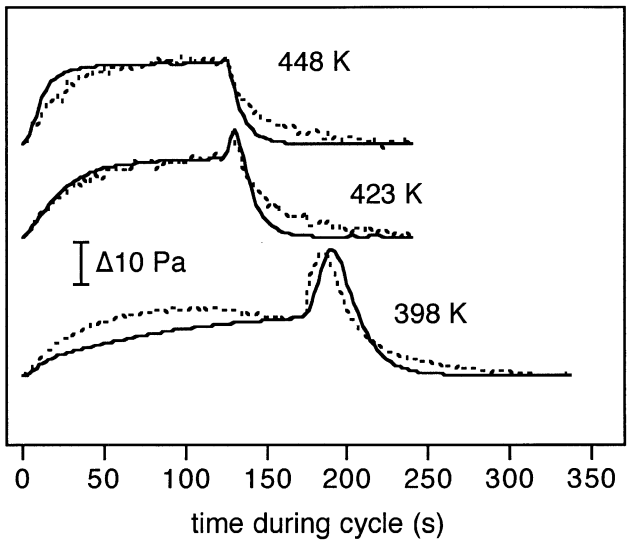

Fig. 5. Centerplane CO_2 responses. Comparison between data (dashed lines) and simulation (solid lines). In Figs. 5–11, the simulation results were computed by numerically integrating Eqs. (1), (6), (7), and (10) for CO and oxygen and two surface site types. The reaction rate terms are given by Eqs. (20)–(24).

6.2. Simulation fit to data

Fig. 5 shows a comparison between the experimental CO_2 responses at the pellet centerplane and the simulated responses given by the model. A slower response was obtained at the lowest temperature, so a longer cycle period was used at this temperature in order to approach steady state at the end of each half cycle.

The mid-cycle CO_2 peak height and its change with temperature is accurately simulated by the model. Another significant achievement of the model is that the mid-cycle CO_2 peak was obtained in the absence of a CO_2 peak at the start of the cycle. The decay of CO_2 in the last half of the cycle is more rapid for the model than for the data. One process that might help to remove this discrepancy is addition to the model of CO_2 adsorption and desorption from the support. Since experiments in this reactor indicated that this process is negligible under our conditions, some other surface processes may have to be explored.

Figs. 6 and 7 show responses at 398 and 448 K, respectively. At 398 K, the CO_2 production rate, which is proportional to the bulk CO_2 pressure, is small during the first half of a cycle, whereas the mid-cycle CO_2 peak in CO_2 production rate is large. Conversely, at 448 K, the CO_2 production rate is relatively large during the first half of a cycle, whereas the mid-cycle CO_2 peak in CO_2 production rate is small.

The biggest difference between the experimental and model responses is during the first half of the cycle at 398 K. The fact that the experimental response goes through a maximum during the first half of the cycle indicates that there is a slow process occurring on the catalyst surface that is causing this slow change in CO_2 level. There are

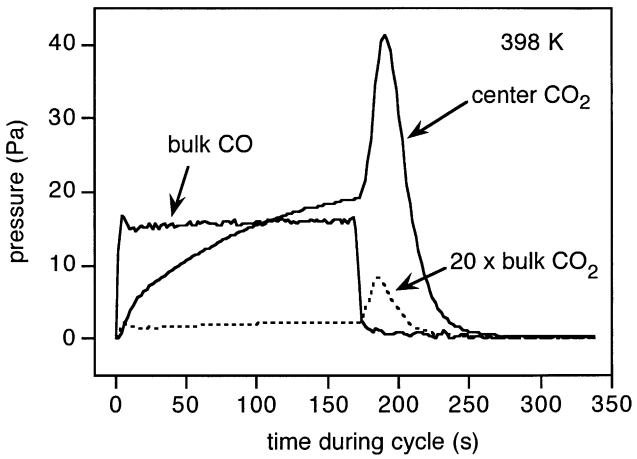

Fig. 6. Reaction responses at 398 K. CO is data, CO_2 is simulation.

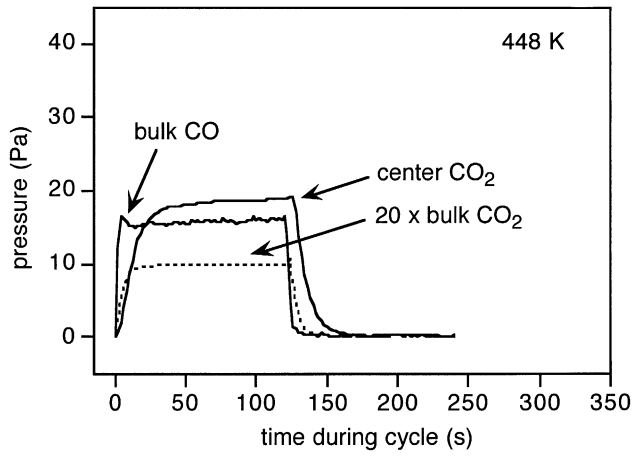

Fig. 7. Reaction responses at 448 K. CO is data, CO_2 is simulation.

several candidates for this slow process: surface reconstruction (Behm, Theil, Norton, & Ertl, 1983; Gruyters, Ali, & King, 1995), change in size of segregated patches of adsorbed CO or O (Gruyters, Ali, & King, 1995; Hoebink et al., 1997), oxidation and reduction of small supported Pt particles (Herz & Shinouskis, 1982; Yeates, Turner, Gellman, & Somorjai, 1985; von Oertzen, Mikhailov, Rotermund, & Ertl, 1996). In each of these processes, the rate of CO_2 formation would tend to go through a maximum at intermediate CO coverages in a manner more strongly dependent on CO coverage than the rate expression for CO_2 formation given above in Eq. (24). We investigated a model in which the rate over one site type varied in a manner used by others to simulate CO surface islands (Graham & Lynch, 1987; Mukesh, Morton, Kenney, & Cutlip, 1984) but obtained no significant improvement.

The parameter values listed in Table 1 are within the ranges of values reported in the literature for this reaction system. Hoebink et al. (1999) fit an elementary-step model to data obtained during periodic switching between O_2 and CO (each at 550 Pa) over Pt/Al_2O_3 particles (0.1–0.15 mm) in a fixed bed reactor over the temperature range 373–433 K. Diffusion resistance was determined to be negligible in these experiments. Their kinetic model differed from the one presented here by having an O_2 adsorption rate that was first order in vacant sites and a description of CO_2 adsorption over the support. An additional step was included that described CO adsorption over O–Pt and reaction with this O–Pt to form CO_2. This step will be discussed below in Section 6.7. The parameter values in Hoebink et al. were $S_{O_2}^{ads} = 5.3 \times 10^{-3}$, $S_{CO}^{ads} = 0.19$, $A_{CO}^{des} = 6 \times 10^{14}\ s^{-1}$, $E_{CO}^{des} = (1.20 - 0.15\ \Theta_{CO}) \times 10^5\ J\ mol^{-1}$, $A^{rxn} = 3.7 \times 10^5\ s^{-1}$, $E^{rxn} = (4.4 - 0.9\ \Theta_{CO}) \times 10^4\ J\ mol^{-1}$. These parameter values are within an order-of-magnitude of those determined here. Considering the complexity of the physical systems, the relative simplicity of the mathematical models, and the differences in the physical systems and models between the two works, this is reasonable agreement. The parameter values reported here and by Hoebink et al. are also within ranges measured over Pt single crystals (Lauterbach et al., 1999).

6.3. CO penetration to pellet center

Penetration of CO to the centerplane in these experiments was not measured in significant amounts. A small centerplane peak in CO shown in Fig. 9 of Cannestra et al. (1997) is believed to result primarily from the mass spectrometer cracking pattern of CO_2. There is evidence in other experiments, such as those shown in Figs. 4 and 5 of Cannestra et al. for appearance of CO in the centerplane chamber after the feed CO is turned off. A very small centerplane CO peak (0.2% of maximum CO pressure), which appears after the feed CO has been turned off, could be obtained in simulations.

6.4. Spatiotemporal patterns

The model's predictions match the concentration responses over both faces of the pellet over a relatively wide temperature range. This indicates that internal patterns predicted by the model are qualitatively reliable.

Figs. 8–10 show predicted spatiotemporal patterns inside the pellet at 398, 423 and 448 K, respectively. In each individual plot in the figures, the vertical axis is position within the pellet (bulk face at top, centerplane face at bottom) and the horizontal axis is time during a cycle. The plot for each variable is normalized using the maximum value of that variable obtained in the three experiments. Gaseous O_2 and adsorbed O atom coverages are not shown. Gaseous O_2 remains at a relatively constant level and the adsorbed O atom pattern is approximately the inverse of the adsorbed CO pattern.

In the top plot in Fig. 8 at 398 K, CO gas penetrates relatively slowly into the pellet during the first half of the

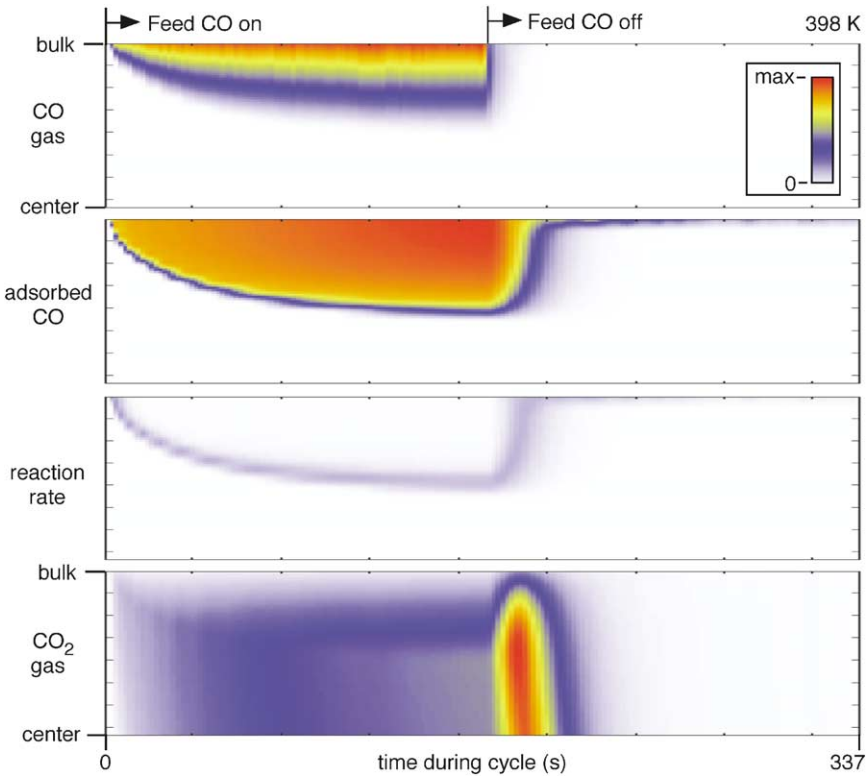

Fig. 8. Predicted patterns in pellet during one cycle at 398 K. Same experiment shown in Fig. 6 and in Fig. 5 at 398 K. For each variable plotted in Figs. 8–10, values at each temperature are normalized to the maximum value obtained for that variable over the entire range of temperature, and the scale bar is linear. At the bulk face just before feed CO is turned off: $\Theta_{1CO} = 0.997$, $\Theta_{1O} = 0.00116$, $\Theta_{2CO} = 0.645$, $\Theta_{2O} = 0.350$.

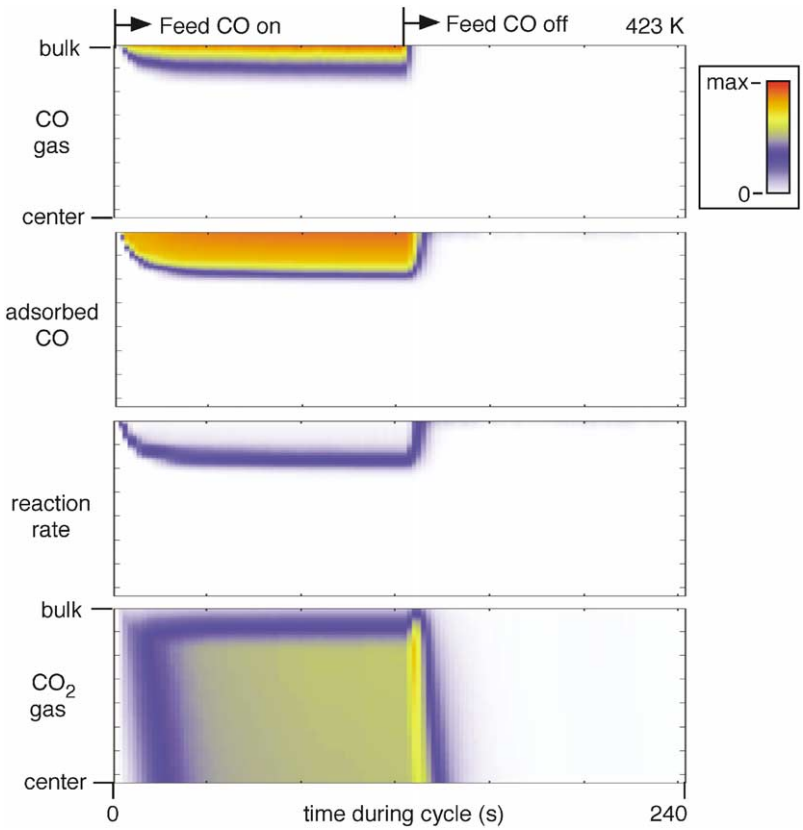

Fig. 9. Predicted patterns in pellet during one cycle at 423 K. Same experiment as shown in Fig. 4 and in Fig. 5 at 423 K.

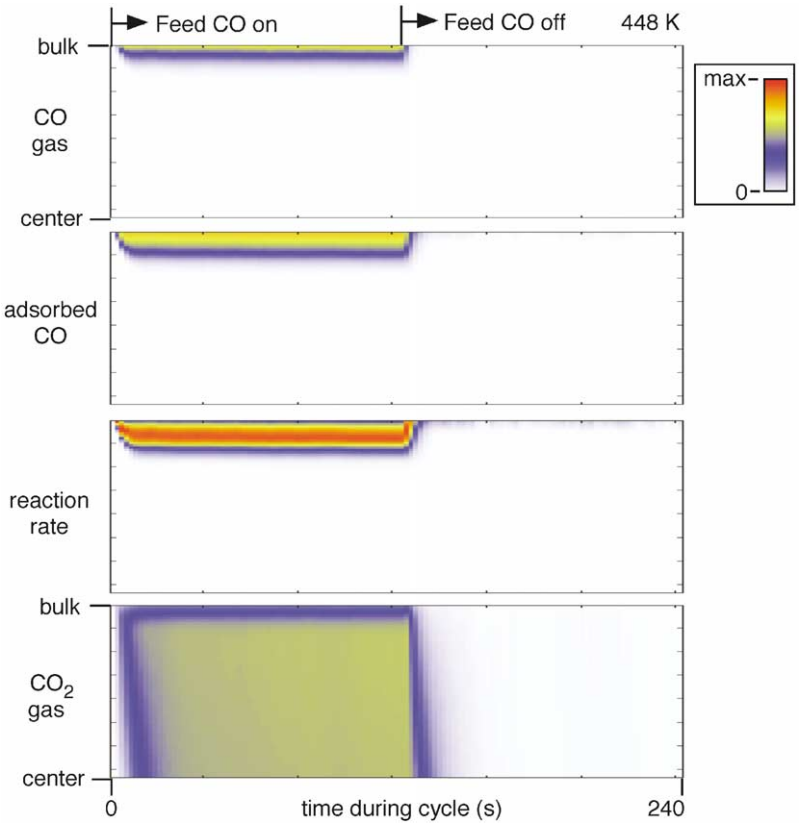

Fig. 10. Predicted patterns in pellet during one cycle at 448 K. Same experiment as shown in Fig. 7 and in Fig. 5 at 448 K.

cycle, and then it rapidly diffuses out of the pellet after the feed CO is turned off at mid cycle. In the second plot from the top, adsorbed CO coverage is high wherever CO gas is present. Because high CO coverages are reached at very low CO pressures, the penetration of adsorbed CO appears at first glance in the plots to be greater than that of CO gas. Relative to CO gas, adsorbed CO is removed relatively slowly after feed CO gas is switched off at mid-cycle.

The third plot in Fig. 8 shows the rate of CO_2 formation, i.e., the local reaction rate. During the first half of a cycle, while the feed CO is flowing, the reaction occurs mainly in the zone at the limit of CO penetration into the pellet, where both adsorbed CO and adsorbed O atom coverages are significant. Just after the feed CO is turned off at mid-cycle and the gaseous CO level drops rapidly everywhere in the pellet, reaction starts to occur everywhere that adsorbed CO is present in the pellet. The rate decays as all adsorbed CO is consumed. The bottom plot in Fig. 8 shows the gaseous CO_2 levels in the pellet.

Just after the feed CO is turned off at mid-cycle and reaction starts to consume the adsorbed CO, the gaseous CO_2 levels rise dramatically. When the feed CO is turned off, CO gas rapidly diffuses from the pellet. The removal of much of the gas-phase CO lowers CO coverages and increases O coverages rapidly such that reaction takes place over the entire length of the pellet through which CO had penetrated. This reaction consumes most of the CO that had been adsorbed by reaction rather than letting it diffuse out of the pellet.

The series of Figs. 8–10 shows what happens inside the pellet as temperature increases:

- the distance of CO penetration into the pellet decreases,
- the amount of CO that is adsorbed inside the pellet just before mid-cycle decreases,
- the maximum local reaction rate increases,
- the location of the maximum local reaction rate moves closer to the bulk face,
- the level of CO_2 produced in the first half of a cycle increases,
- the peak in CO_2 just after mid-cycle decreases in size, and
- the rate of approach to steady state increases.

6.5. *Mid-cycle* CO_2 *peak*

The CO_2 peak that appears after the feed CO is turned off is due to desorption and reaction of the adsorbed CO that has accumulated within the pellet during the first half of a cycle. Since the CO surface coverage is high wherever CO gas is present, the amount of adsorbed CO that has accumulated on the surface also is reduced by the decreased penetration of CO gas into the pellet at higher temperature. At a constant local CO pressure, the reduction in local CO coverage by

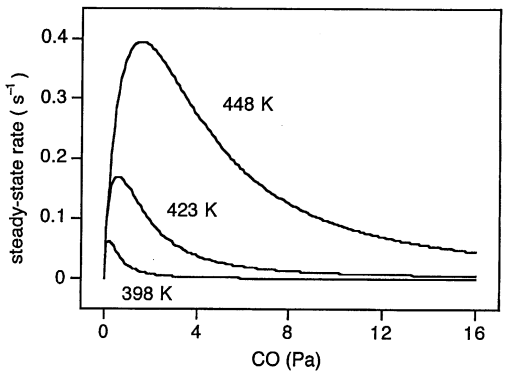

Fig. 11. Steady-state reaction rate at constant O_2 pressure of 110 Pa, from model.

increased temperature is relatively small. This reduction in local CO coverage by the shift in CO adsorption equilibrium is a minor direct contributor to the reduced storage of CO in the pellet at higher temperature and the reduced size of the CO_2 peak.

The major reason for the decreased storage of CO in the pellet is the decreased penetration of CO into the pellet. Because the rate of reaction has increased much more than the rate of diffusion as the temperature was increased, CO is present over a smaller length of the pellet, so less can be stored.

The reduced storage of CO in the pellet at higher temperature and the reduced size of the CO_2 peak is a result of the coupling between adsorption equilibrium, reaction rate, and diffusion resistance within the porous pellet. This coupling is described by the following sequence of processes:

- The reduction in local CO coverage by the shift in CO adsorption equilibrium reduces CO inhibition of the reaction rate.
- This reduced CO inhibition, along with the increase in surface reaction rate coefficient with temperature, leads to an increase in the reaction rate with temperature.
- The increase in reaction rate with temperature, relative to the increase in diffusion rate, then results in decreased penetration of CO gas into the pellet.

Finally, the decreased penetration of CO gas into the pellet results in decreased storage of adsorbed CO in the pellet, which is the primary reason for the decreased CO_2 peak at higher temperature.

6.6. Steady-state reaction

Steady-state conditions were closely approached just before the CO feed was turned off during the cycling experiments. Fig. 11 show plots of the steady-state reaction rates predicted by the model at a constant O_2 pressure of 110 Pa. The plots show the known inhibitory effects of relatively high CO pressure on the reaction rate. As temperature increases, the rate at each CO pressure increases, and the location of the maximum in rate vs. CO pressure shifts to higher CO pressures. Using a model with similar kinetic behavior, Wei and Becker (1975) demonstrated the potential for effectiveness factors greater than 1 in CO oxidation. Such high effectiveness factors were observed experimentally here.

Table 2 summarizes conditions at mid cycle just before CO was turned off. The effectiveness factor value in the second row is the ratio of the numbers in the third and fourth rows, i.e., the overall rate obtained divided by the rate that would have been obtained if all Pt in the pellet were exposed to bulk conditions. The effectiveness factor values are greater than 1 at all three temperatures: the reaction rate is enhanced by diffusion resistance. This is because the rate obtained under the relatively high bulk CO pressure is in the kinetic regime in which high CO pressure and, thus, high CO surface coverages inhibit O_2 adsorption and reaction. The lower CO pressures inside the pellet caused by diffusion resistance results in lower inhibition and higher reaction rates. The effectiveness factor decreases as temperature increases primarily because inhibition of the reaction by adsorbed CO decreases.

Table 2 shows that the apparent activation energy of the overall rate is approximately one-half the activation energy of the rate that would be obtained with all sites under the bulk CO pressure value, i.e., the "true" or "intrinsic" rate at bulk conditions. Reduction of a reaction's apparent activation energy to approximately one-half of the "true" value by strong diffusion resistance is shown analytically for nth order reactions ($n > -1$) in standard texts (Froment & Bischoff, 1990).

The last row of Table 2 confirms that CO penetration into the pellet is reduced as temperature increases. This reduced penetration of CO into the pellet is a result of the increased effect of diffusion resistance: as temperature increases, the rate of reaction increases much more than the rate of diffusion increases.

Because of the inhibition of the reaction by CO and the intrapellet diffusion resistance, reaction under the quasi-steady-state conditions at mid cycle occurs in a narrow zone in the interior of the pellet. Approximately the same overall rate could be obtained if Pt were located only within the narrow zone in which reaction occurs, thus optimizing the rate per Pt atom. Several works have discussed the optimal distribution of active sites within a catalyst pellet for CO oxidation (Wei & Becker, 1975) and other reactions (Gavriilidis, Varma, & Morbidelli, 1993; Papageorgiou, Price, Gavriilidis, & Varma, 1996).

6.7. Participation of the two site types

The experimental behavior most difficult to simulate was (a) to have the absence of a peak in centerplane CO_2 when the CO was turned on at the start of a cycle and then (b) to obtain a peak in centerplane CO_2 peak after feed CO

Table 2
Mid-cycle conditions

Temperature	398 K	423 K	448 K
Effectiveness factor	11	3.0	1.4
Overall rate (mol s^{-1}) $\Delta E_{apparent} = 6.3 \times 10^4$ J mol^{-1}	5.1×10^{-11}	1.2×10^{-10}	4.3×10^{-10}
Rate if all sites under bulk conditions (mol s^{-1}) $\Delta E_{apparent} = 1.2 \times 10^5$ J mol^{-1}	4.5×10^{-12}	4.1×10^{-11}	3.1×10^{-10}
Fractional distance into pellet of CO gas penetration to CO $< 1\%$ of bulk	0.58	0.32	0.26

These are conditions obtained in the catalyst pellet as the pellet closely approached steady-state conditions just before the CO feed gas was turned off during periodic switching of CO on–off in a constant flow of O_2.

was turned off at mid cycle. This behavior indicates that the amount of adsorbed oxygen that is reacted off the surface at the start of a cycle is much less than the amount of CO that accumulates and then is reacted off the surface in the second half of the cycle. The two-site model used in this work shows this behavior by the action of site 2, which primarily acts to adsorb and store CO on the surface during the first half of a cycle, then releases it during the last half of the cycle. CO adsorbs on site 2 in the first half of a cycle and accumulates without reacting with significant amounts of the oxygen present on these sites. Most of the CO released by site 2 in the second half of the cycle readsorbs on site 1 and reacts to form most of the CO_2 that appears in the mid-cycle CO_2 peak. The behavior over the two site types is not simply additive because of this coupling through gas-phase CO.

The main contribution of site 2 to the responses was to adsorb CO during the first half of a cycle and then release it after feed CO was switched off. The main difference in parameter values between the two site types in the model was that the reaction rate coefficient for site 2 is much less than for site 1. The simulation results show that, although site type 1 represents only 15% of the total sites, over 90% of the CO_2 is formed over these sites. A second difference is that the desorption rate coefficient values were higher for site 2. Since the sticking coefficients and, therefore, the adsorption rate coefficients were the same over the two sites, the increased desorption rate coefficient over site 2 indicates that CO is adsorbed less strongly over site 2.

Possible alternatives for site and activity distributions over supported Pt particles were discussed by Racine and Herz (1992). Both the lower activity for reaction and the weaker CO adsorption over site 2 are consistent with site 2 representing an oxidized form of Pt. Pt, when exposed to O_2 at relatively high pressures can become oxidized or incorporate subsurface O (Sales, Turner, & Maple, 1982; Peuckert & Bonzel, 1984; Yeates et al., 1985; von Oertzen et al., 1996; Thundat & Maya, 1999), especially when dispersed as small particles over oxide supports (Yao, Sieg, & Plummer, 1979; Herz & Shinouskis, 1982; Konigsberger & Sayers, 1985; Volter, Lietz, Spindler, & Lieske, 1987; McCabe, Wong, & Woo, 1988; Lin, Davis, & Fripiat, 1990; van Neer & Bliek, 1999). The catalyst sample was pretreated by exposure to air at 773 K and atmospheric pressure, then partially reduced by exposure to CO and H_2 at low pressures. In addition, O_2 flow was continuous over the sample during experimentation whereas CO flow was only periodically turned on during data collection. Thus, we propose that site 2 represents oxidized Pt sites in this catalyst sample.

The model of Hoebink et al. (1999) includes a step that describes CO adsorption over adsorbed O and reaction with this Pt-O to form CO_2. The inclusion of this step can be interpreted in several ways, one of which would make it similar to site 2 in our model. The literal interpretation is that an Eley–Rideal mechanism for CO_2 formation exists. A second interpretation is that this Pt-O-CO physically corresponds to a compressed, coadsorbed layer of Pt-O and Pt-CO (Engel & Ertl, 1979) and has the effect of causing CO adsorption and reaction rates in the model to have coverage-dependence on adsorbed O. Since the CO adsorption equilibrium coefficient is lower over Pt-O-CO than over Pt-CO, and since the reaction rate is lower for Pt-O-CO than for Pt-O + Pt-CO in Hoebink et al., a third interpretation might be that their Pt-O-CO structure is similar to CO adsorption and reaction over our site 2.

The contribution of site 2 occurs primarily during transients. This means that steady-state measurements alone would not reveal the presence of the proposed bimodal distribution of sites.

6.8. Approach to CO adsorption equilibrium

The model describes the adsorption and desorption steps for CO separately and makes no assumptions about approach to adsorption equilibrium. Such assumptions are routinely made in most steady-state models of CO oxidation. This assumption was not made in the model because conditions varied over wide ranges within the pellet and also varied dynamically as conditions changed with time. This separate description of nonequilibrium CO adsorption and desorption rates increased the stiffness of the system of equations dramatically and, thus, increased the computation times.

The simulations showed that the CO adsorption rate exceeded the desorption rate by as much as 100% at very early time near the outer surface of the pellet. During the first half of a cycle, the adsorption rate exceeded the desorption rate by approximately 20% at edge of the propagating CO front. At other times and locations, the adsorption and desorption rates were nearly equal. Analysis of the simulation results shows that the surface reaction rate is only 2% or less of adsorption rate at all places and times. Thus, the difference between the adsorption and desorption rates is primarily due to transient filling and emptying of surface sites with adsorbed CO. During simulation of the CO adsorption–desorption response experiments, only small differences were obtained between a model that specified quasi-equilibrium adsorption and a model that described separate adsorption and desorption rates. When compared with steady-state rates predicted by the nonequilibrium model, which are shown in Fig. 11, steady-state rates calculated with an assumption of quasi-equilibrium CO are 10–15% lower in magnitude and show a maximum in rate vs. CO pressure at a slightly lower CO pressure.

In the model of Hoebink et al. (1999), CO desorption and CO reaction rate coefficients are within an order-of-magnitude of each other, indicating that CO equilibrium was not closely approached in their simulations. If the CO sticking coefficient used here were reduced from 1 to the value of 0.186 used by Hoebink et al. with the ratio of adsorption and desorption rate coefficients kept constant, then our desorption rate coefficients would come within an order-of-magnitude of our CO reaction rate coefficient and would cause a greater deviation from adsorption equilibrium.

We conclude that, for this sample under these conditions, assumption of quasi-equilibrium CO adsorption would be a good first approximation. The advantage of this approximation is that computation time for a run would decrease by an estimated factor of 4–6, allowing faster model development and parameter estimation. Detailed computations without this approximation could then be done for final simulations.

6.9. Computation time

Several factors contributed to long computation times:

- the separate description of nonequilibrium CO adsorption and desorption rates,
- the large surface-to-gas capacity ratio, α, and
- the persistence of measured transients for long experimental times.

The first factor has been discussed above. With respect to the surface-to-gas capacity ratio, α, there is a trade-off involved. The advantage of a high value is that experimental responses are more sensitive to and, thus, provide more information about surface processes such as accumulation of adsorbed species on the surface. The disadvantage is that a high value of the surface-to-gas capacity ratio increases the stiffness of the equations describing the system. In this work, at 398 K, $\alpha_{CO} = 590$. This value could be reduced significantly in order to reduce computation time while retaining sensitivity to surface processes. The value of α could be reduced experimentally by reducing the active site concentration in the sample and increasing reactant pressures.

Surface processes inherent to the surface chemistry of a sample, such as surface reconstruction or oxidation, can also affect the experimental response time and, thus, the length of computations required in the simulation. The results at 398 K in the first half of the cycle indicate that slow surface processes may be occurring in this sample.

7. Conclusions

The dynamic single-pellet diffusion reactor is useful for studying the processes of diffusion, adsorption, and reaction under dynamic conditions. Diffusion coefficients and adsorption behavior can be measured over the same sample used for reaction studies. In addition to porous catalyst pellets, other one-dimensional samples of porous materials can be studied.

A model with standard Langmuir–Hinshelwood kinetics, with the additional specification of a bimodal distribution of sites was developed. This model provided a quantitative fit over a 50 K temperature range to the quasi-steady-state reaction rate and the transient CO_2 production peak that occurred following shut-off of the feed CO. Both the model and the experimental data showed the presence of significant concentration gradients in the pellet.

CO penetration into the pellet was retarded by diffusion resistance. Reaction occurred in a thin zone within the pellet at the edge of CO penetration, except when feed CO was turned off and reaction occurred everywhere throughout the part of the pellet through which CO had penetrated. This rapid spread of the reaction due to reduced CO inhibition caused the large peak in CO_2 production. The change in size of this peak with temperature resulted from coupling between adsorption equilibria, reaction rate, and diffusion resistance.

The model indicated that the surface reaction step was rate-limiting throughout the entire range of dynamic conditions. The model also provided an understanding of the complex interactions between diffusion, adsorption, and reaction that occur during dynamic operation of the catalyst.

Notation

A	area of plane face of pellet, m^2
A_n	pre-exponential factor in Arrhenius expression for k_{ni}^{des} and k_n^{rxn}, s^{-1}

C_i concentration of gaseous species i in pellet pores, mol m^{-3}

C_i^{cp} concentration of gaseous species i in centerplane chamber, mol m^{-3}

C_{ni}^{surf} concentration over site type n in pellet of surface species i, mol m^{-3}

C_{tot}^{surf} concentration of surface Pt atoms in pellet, mol m^{-3}

D_i^{eff} effective diffusion coefficient of species i in pellet, m^2 s^{-1}

E_n activation energy in Arrhenius expression for k_{ni}^{des} and k_n^{rxn}, J mol^{-1}

k_{ni}^{ads} rate coefficient for adsorption over site type n of species i, m^3 mol^{-1} s^{-1}

k_{ni}^{des} rate coefficient for desorption over site type n of species i, s^{-1}

k_n^{rxn} rate coefficient for surface reaction over site type n, s^{-1}

L thickness of pellet, m

M_i molecular weight of species i, kg mol^{-1}

Q_i^{cpl} pumping speed of species i through centerplane chamber leak, m^3 s^{-1}

r_i total rate, summed over all site types, for species i, s^{-1}

r_{ni} rate over site type n for species i, s^{-1}

R ideal gas constant, 8.314 kg m^2 mol^{-1} K^{-1} s^{-2}

S_i^{ads} adsorption sticking probability of gaseous species i colliding with empty surface

t time, s

T temperature, K

V^{cp} volume of centerplane chamber, m^3

Greek letters

α_i surface-to-gas capacity ratio for species i

$\Delta E_{apparent}$ apparent activation energy, J mol^{-1}

ε void fraction of pellet

Θ_{ni} fraction of surface site type n covered by adsorbed species i

κ constant in adsorption rate expression for O_2

λ dimensionless position within pellet

σ area occupied by one mole of surface Pt atoms, m^2 mol^{-1}

τ_i characteristic time for diffusion of gaseous species i in absence of adsorption in pellet pores, s

τ_i^{cpl} characteristic time for flow of species i out of centerplane chamber through sample leak, s

τ_i^{cpp} characteristic time for diffusion of species i into centerplane chamber from pellet, s

ϕ_n fraction of surface sites which are of type n

Ψ_i dimensionless concentration of gaseous species i in pellet pores

Ψ_i^{cp} dimensionless concentration of gaseous species i in centerplane chamber

Acknowledgements

Richard Hopfinger, a visiting student from Ecole Nationale Supérieure d'Electrochimie et d'Electrométallurgie de Grenoble, assisted with some of the experimental work.

References

Au, S. S., Dranoff, J. S., & Butt, J. B. (1995). Nonuniform activity distribution in catalyst particles—benzene hydrogenation on supported nickel in a single pellet diffusion reactor. *Chemical Engineering Science*, *50*, 3801–3812.

Behm, R. J., Theil, P. A., Norton, P. R., & Ertl, G. (1983). The interaction of CO and Pt(100). I. Mechanism of adsorption and Pt phase transition. *Journal of Chemical Physics*, *78*, 7437.

Cannestra, A. F., Nett, L. C., & Herz, R. K. (1997). Measurement of gas composition at the center of a porous pellet during adsorption and catalytic reaction under dynamic conditions. *Journal of Catalysis*, *172*, 346–354.

Cho, B. K. (1983). Dynamic behavior of a single catalyst pellet 1. Symmetric concentration cycling during carbon monoxide oxidation over platinum/alumina. *Industrial and Engineering Chemistry Fundamentals*, *22*, 410–420.

Crank, J., & Nicolson, P. (1947). A practical method for numerical evaluation of solutions of partial differential equations of the heat-conduction type. *Proceedings of the Cambridge Philosophical Society, Mathematical and Physical Sciences*, *43*, 50–67.

Dekker, F. H. M., Klopper, G., Bliek, A., Kapteijn, F., & Moulijn, J. A. (1994). Transient kinetics of heterogeneous catalysts—CO oxidation over supported Cr and Cu. *Chemical Engineering Science*, *49*, 4375–4390.

Dekker, F. H. M., Nazloomian, J. G., Bliek, A., Kapteijn, F., Moulijn, J. A., Coulson, D. R., Mills, P. L., & Lerou, J. J. (1997). Carbon monoxide oxidation over platinum powder: A comparison of TAP and step-response experiments. *Applied Catalysis A—General*, *151*, 247–266.

Dogu, T., Yasyerli, N., Mccoy, B. J., & Smith, J. M. (1996). One-sided single-pellet technique for adsorption and intraparticle diffusion. *A.I.Ch.E. Journal*, *42*, 516–523.

Engel, T., & Ertl, G. (1979). Elementary steps in the catalytic oxidation of carbon monoxide on platinum metals. *Advances in Catalysis*, *28*, 1–78.

Ertl, G., Neumann, M., & Streit, K. M. (1977). Chemisorption of CO on the Pt(111) Surface. *Surface Science*, *64*, 393.

Farrauto, R., & Heck, R. (1999). Catalytic converters: State of the art and perspectives. *Catalysis Today*, *51*, 351.

Foger, K. (1984). Dispersed metal catalysts. *Catalysis Science and Technology*, *6*, 227.

Froment, G. F., & Bischoff, K. B. (1990). *Chemical reactor analysis and design* (2nd ed.). New York: Wiley.

Gavriilidis, A., Varma, A., & Morbidelli, M. (1993). Optimal distribution of catalyst in pellets. *Catalysis Reviews—Science and Engineering*, *35*, 399–456.

Gleaves, J. T., Ebner, J. R., & Kuechler, T. C. (1988). Temporal analysis of products (TAP)—a unique catalyst evaluation system with submillisecond time resolution. *Catalysis Reviews—Science and Engineering*, *30*, 49–116.

Graham, W. R. C., & Lynch, D. T. (1987). Island models and the catalytic oxidation of carbon monoxide. *Surface Science*, *187*, L633–L638.

Gruyters, M., Ali, T., & King, D. A. (1995). Modelling temporal kinetic oscillations for CO oxidation on Pt(100). The (1×1)-CO island growth rate power law model. *Chemical Physics Letters*, *232*, 1–6.

Guinn, K. V., Rhoades, D. S., & Herz, R. K. (1997). Thermal desorption over wide pressure ranges applied to characterization of equilibrium adsorption of CO over Pt. *Surface Science*, *393*, 47–63.

Gulari, E., Zhou, X., & Sze, C. (1995). Catalytic oxidation of carbon monoxide under periodic and transient operation. *Catalysis Today*, *25*, 145–157.

Hegedus, L. L., & Petersen, E. E. (1974). *Catalysis Reviews—Science and Engineering*, *9*, 245.

Herz, R. K. (1987). Dynamic behavior of automotive three-way emission control systems. *Studies in Surface Science and Catalysis*, *30*, 427–444.

Herz, R. K., Kiela, J. B., & Marin, S. P. (1982). Adsorption effects during temperature-programmed desorption of carbon monoxide from supported platinum. *Journal of Catalysis*, *73*, 66–75.

Herz, R. K., & Marin, S. P. (1980). Surface chemistry models of carbon monoxide oxidation on supported platinum catalysts. *Journal of Catalysis*, *65*, 281–296.

Herz, R. K., & Shinouskis, E. J. (1982). Transient oxidation and reduction of alumina-supported platinum. *Applications of Surface Science*, *19*, 373–397.

Hindmarsh, A. C., & Johnson, S. H. (1991). Dynamic simulation of multispecies reaction diffusion in nonisothermal porous pellets. *Chemical Engineering Science*, *46*, 1445–1463.

Hlavacek, V., & Van Rompay, P. (1981). *Chemical Engineering Science*, *36*, 1587–1597.

Hoebink, J. H. B. J., Huinink, J. P., & Marin, G. B. (1997). A quantitative analysis of transient kinetic experiments: The oxidation of CO by O_2 over Pt. *Applied Catalysis A—General*, *164*, 139–151.

Hoebink, J. H. B. J., Nievergeld, A. J. L., & Marin, G. B. (1999). CO oxidation in a fixed bed reactor with high frequency cycling of the feed. *Chemical Engineering Science*, *54*, 4459–4468.

Jirát, Stepánek, Kubícek, , & Marek, (1998). Nonstationary operation of a system of catalytic monolithic reactors for selective NO_x reduction. *Chemical Engineering Science*, 54, 2609–2618.

Kaul, D. J., Sant, R., & Wolf, E. E. (1987). Integrated kinetic modeling and transient FTIR studies of carbon monoxide oxidation on platinum/silica. *Chemical Engineering Science*, *42*, 1399–1411.

Keller II, G. E. (1995). Adsorption. *Chemical Engineering Progress*, 56–67.

Khadilkar, M. R., Al-Dahhan, M. H., & Dudukovic, M. P. (1998). Parametric study of unsteady-state flow modulation in trickle-bed reactors. *Chemical Engineering Science*, *54*, 2585–2595.

Kisliuk, P. (1957). The sticking probabilities of gases chemisorbed on the surfaces of solids. *Journal of Physics and Chemistry of Solids*, *3*, 95–101.

Kisliuk, P. (1958). The sticking probabilities of gases chemisorbed on the surfaces of solids—II. *Journal of Physics and Chemistry of Solids*, *5*, 78–84.

Kobayashi, M., Maeda, Y., & Takahashi, N. (1983). Discrimination of rival kinetic models in heterogeneous catalysis by the dynamic behavior of products. *Journal of Chemical Technology and Biotechnology, Chemical Technology*, *33A*, 219–226.

Konigsberger, D. C., & Sayers, D. E. (1985). *Solid State Ionics*, *16*, 23–27.

Lauterbach, J., Bonilla, G., & Pletcher, T. D. (1999). Non-linear phenomena during CO oxidation in the bar pressure range: A comparison between Pt/SiO_2 and Pt(100). *Chemical Engineering Science*, *54*, 4501–4512.

Lin, X., Davis, J., & Fripiat, J. J. (1990). Thermodynamics of reduction and oxidation reactions on oxidized and reduced Pt supported on $\gamma - Al_2O_3$. *Catalysis Letters*, *6*, 1–12.

McCabe, R. W., Wong, C., & Woo, H. S. (1988). *Journal of Catalysis*, *114*, 354.

Mukesh, D., Morton, W., Kenney, C. N., & Cutlip, M. C. (1984). *Surface Science*, *138*, 237.

Oh, S. H., & Hegedus, L. L. (1982). Dynamics of high-temperature carbon monoxide chemisorption on platinum–alumina by fast-response IR spectroscopy. In *Catalysis under transient conditions, American Chemical Society Symposium Series*, Vol. 178, p. 79 (Chapter 4).

Papageorgiou, P., Price, D. M., Gavriilidis, A., & Varma, A. (1996). Preparation of Pt/γ-Al_2O_3 pellets with internal step-distribution of catalyst—experiments and theory. *Journal of Catalysis*, *158*, 439–451.

Peuckert, M., & Bonzel, H. P. (1984). *Surface Science*, *145*, 239.

Pozrikidis, C. (1998). *Numerical computation in science and engineering*. Oxford: Oxford University Press.

Racine, B. N., & Herz, R. K. (1992). Modeling dynamic CO oxidation over Pt/Al_2O_3: Effects of intrapellet diffusion and site heterogeneity. *Journal of Catalysis*, *137*, 158–178.

Russell, N. M., & Ekerdt, J. G. (1996). *Surface Science*, *364*, 199.

Sales, B. C., Turner, J. E., & Maple, M. B. (1982). Oscillatory oxidation of CO over Pt, Pd, and Ir catalysts: Theory. *Surface Science*, *114*, 381.

Sant, R., & Wolf, E. E. (1990). Elementary-step modeling and transient FTIR studies of CO oxidation on Rh/SiO_2. *Chemical Engineering Science*, *45*, 3137–3147.

Silveston, P. L., Hudgins, R. R., Bogdashev, S., Vernijakovskaja, N., & Matros, Y. S. (1994). Modelling of a periodically operating packed-bed SO_2 oxidation reactor at high conversion. *Chemical Engineering Science*, *49*, 335–341.

Tamaru, K. (1991). Dynamic relaxation methods in heterogeneous catalysis. *Catalysis—Science and Technology*, *9*, 87–130.

Thundat, T., & Maya, L. (1999). Monitoring chemical and physical changes on sub-nanogram quantities of platinum dioxide. *Surface Science*, *430*, L546.

van Neer, F., & Bliek, A. (1999). The feedback mechanism in self-oscillations for CO oxidation over EUROPT-3. *Chemical Engineering Science*, *54*, 4483–4499.

Volter, J., Lietz, G., Spindler, H., & Lieske, H. (1987). *Journal of Catalysis*, *104*, 375.

von Oertzen, A., Mikhailov, A., Rotermund, H.-H., & Ertl, G. (1996). Subsurface oxygen formation on the Pt(110) surface: Experiment and mathematical modeling. *Surface Science*, *350*, 259.

Wei, J., & Becker, E. R. (1975). The optimum distribution of catalytic material in automotive catalysis. *American Chemical Society Symposium Series*, *143*, 116–132.

Weinberg, W. H., Comrie, C. M., & Lambert, R. M. (1976). Kinetics of adsorption of CO on Group VIII transition metals. *Journal of Catalysis*, *41*, 489.

Yao, H. C., Sieg, M., & Plummer, H. K. (1979). *Journal of Catalysis*, *59*, 365.

Yeates, R. C., Turner, J. E., Gellman, A. J., & Somorjai, G. A. (1985). The oscillatory behavior of the CO oxidation reaction at atmospheric pressure over platinum single crystals: Surface analysis and pressure dependent mechanisms. *Surface Science*, *149*, 175–190.

Zagoruiko, A. N., Matros, Y. S., Kumar, V. R., & Kulkarni, B. D. (1992). Reactor performance with periodic flow reversal for a multistep complex reaction. *Chemical Engineering Science*, *47*, 4315–4321.